J. Plasma Fusion Res. SERIES, Vol. 11 (2015)

Evaluation Study of Source Term for Severe Accident Analysis of Molten Salt Reactors

Michio YAMAWAKI*[a], Yuji ARITA[a], Ken-ichi FUKUMOTO[a], Masami TAIRA[b] and Ryota FUJIMURA[b]

[a] *Research Institute of Nuclear Engineering, Univ. of Fukui, Tsuruga, Fukui, 914-0055, Japan*
[b] *Graduate School of Nuclear Power and Energy Safety Engineering, Univ. of Fukui, Fukui, 914-0055, Japan*

(Received: 24 September 2014 / Accepted: 19 January 2015)

Source term for severe accident analysis of molten salt reactors (MSRs) has been investigated as part of preliminary studies to develop MSRs. As a severe accident of MSRs, exposure of heated fluoride fuel molten salt to atmosphere was assumed to take place. Vaporization of fluoride molten salt was studied by means of the Knudsen effusion mass spectrometry for pseudo-binary fluoride systems to clarify the behaviors of cesium and iodine in the fluoride molten salt. Besides, corrosion of nickel-based Hastelloy-N, candidate alloy for the structural material of MSRs, was investigated metallographically. In these studies, emphasis was laid on the interactions among molten fluoride, fission products and atmosphere. From the studies, a lot of useful information related to the source term for MSRs have been obtained. This work suggests how to tackle the problem to establish the source term for severe accident analysis of MSRs.

Keywords: molten salt reactor(MSR), thorium, severe accident, source term, FLiNaK, fluoride, vapor pressure measurement, Knudsen effusion mass spectrometry, Hastelloy-N alloy, corrosion

1. Introduction

It is an important subject to carry out the processing and disposal of the fuel debris taken out of the damaged Fukushima Daiichi Reactors as well as the high level radioactive wastes originating from the nuclear power plants. Together with fast reactors and accelerator-driven subcritical systems, which the Japanese Government is supporting financially, molten salt reactors (MSRs) should be also supported by the Government for their development. This is because MSRs are inherent safe reactors and can be used to substantially decrease the amount of high level radioactive waste including the fuel debris from the damaged Fukushima Reactors as well or in better ways. Relevant fission products such as cesium and iodine can be kept thermodynamically stable in the fluoride molten salt so that the severe accidents such as occurred in light water reactors will not take place in MSRs. In this work, a hypothetical severe accident has been assumed to occur in MSRs and the vaporization behavior of fluoride molten salt containing fission product (FP), cesium or iodine, was investigated as to the vapor species and vapor pressures. Further, the corrosion of structural material candidate, Hastelloy-N, by molten salt has been investigated.

There have been considerable interest in molten salt because of their uses as coolant [1], as heat transfer media, and as thermal storage media in many energy-related applications, which are due to their high volumetric heat capacity. MSRs use fluoride salts as nuclear fuel as well as coolant, while High-temperature reactors cooled with fluoride salt (FHRs) use molten fluoride salts as coolant. These salts have a high boiling temperature and high solubility of many FPs. MSRs, original one was developed at Oak Ridge National Laboratory during 1950–1970, are intended for operation at 650°C or higher temperatures[2, 3]. Under the program of Molten Salt Reactor Experiment (MSRE), a 7.5 MW molten salt reactor with uranium fuel dissolved in a molten fluoride salt, was built and was operated at 650°C. Corrosion of structural materials in molten fluoride salt is an important issue in MSR and FHR operation [4]. Hastelloy-N, a relatively low Cr content alloy with Mo addition, was developed for the MSRE program, exclusively for applications using molten fluoride salt. Its corrosion in molten salt was strongly suppressed: corrosion depth at 560/700°C reached only ~100μm within nine years [3, 4]. This alloy must be code-certified for use at the high temperatures required for MSRs and FHRs. Accordingly, corrosion testing and evaluation of all materials in molten salt at temperatures of MSRs and FHRs are required and are conducted as part of FHR development programs all

---

author's e-mail: yamawaki@u-fukui.ac.jp

over the world.

Resistance of structural materials against deterioration due to a beyond-design-basis accident in a nuclear power plant is a consideration in the development of nuclear reactor materials and in the design of advanced nuclear reactors such as the molten salt breeder reactor in the GEN-IV program. This property ensures safety and prevents severe accidents. For example, the cladding material of a PWR should be requested to be ideally strengthened to increase their melting point and to suppress hydrogen gas formation during core melting due to a LOCA incident. In the case of MMSRs or FHRs, emission of fuels and volatile FPs due to leakage of molten salt in a LOCA incident poses hazards. The engineering design of a FHR should prevent extensive damage caused by heavy corrosive attack during a severe accident and prevent deterioration of the interaction between structural materials and molten salt coolant in air. In the present work, the effect of ambient conditions on the corrosion behavior of structural material in molten salt coolant containing FP elements was investigated to evaluate the safety of Hastelloy-N, a structural material for MSR and FHR cores. The molten salt FLiNaK was used instead of FLiBe in this work.

2. Vaporization study of fluoride molten salt

Release of radioactive material to atmosphere in case of a hypothetical severe accident of MSRs such as breaking of a main fuel pipe was studied from the viewpoint of vaporization behavior of molten salt mixture. Identification of the vapor species and measurement of the vapor pressure of molten salt mixture have been performed with the high temperature mass spectrometry,

2.1 Experimental

Anhydrous salts of LiF, LiI and CsF with 99.99% purity each were purchased from Kojundo Chemical Laboratory Co. LTD. LiF-LiI (0, 25, 50, 70 and 100 mol% LiI) mixed salts and LiF-CsF (0, 25, 50, 75 and 100 mol% CsF) mixed salts were prepared by mixing each salt in a tungsten crucible and then heating at 973K in vacuum.

The vapor pressures of the mixed salts were measured using a quadrupole mass spectrometer (Pfeiffer Vacuum QMG700) with a Knudsen cell [5, 6]. The Knudsen cell was made of tungsten, and had an internal diameter of 8 mm, and a height of 10 mm. The diameter of the effusion orifice was 0.3 mm. The electron energy used to ionize the gaseous species was set to 22 eV. The absolute vapor pressure of each species was determined by comparing the intensity of its ionic current (I) with that of LiF vapor over pure LiF. The correlation factor is denoted k in eq.(1). The partial pressure was calculated using the equation

$$P_i = \frac{1}{\sigma_i \gamma_i S_i \Delta E_i} \cdot k\, I_i T \qquad (1)$$

where σ is the ionization cross section, γ is the isotope abundance ratio, S is the relative multiplier gain, ΔE is the electron beam energy minus the appearance potential, T is the absolute temperature, and subscript i denotes the measured gas species, respectively. The ionization cross-section of Li, F, I and Cs atomic vapor species each was taken from the report given by Mann [7]. The relative multiplier gain was calculated by assuming the inverse proportionality to the square root of the mass of the vaporizing species [8].

2.2 Results and discussion

Gaseous species and ionization efficiency curves

Li^+, LiF^+ Li_2F^+, LiI^+, I^+ and I_2^+ were identified as the predominant vapor species over LiF-LiI systems, while Li^+, LiF^+ Li_2F^+ and Cs^+ were detected over LiF-CsF systems. The results are shown in Figs. 1 and 2. The ionization efficiency curves for each species were obtained for ionization energies from 10 to 30 eV. By linear extrapolation of the ionization efficiency curves to zero intensity, the appearance potentials of the above species were determined as shown in Table 1. To provide a sufficiently high ion current, an electron ionization energy of 22 eV was chosen for the measurements.

From a thermodynamic calculation using MALT database and "gem" program [9], the intrinsic gas species are LiF and $(LiF)_2$ for LiF, and LiI, $(LiI)_2$ for LiI and CsF and $(CsF)_2$ for CsF. Therefore, Li^+ (or Cs^+) and Li_2I^+ were considered to be created as follows:

$$LiI + e^- \rightarrow Li^+ + I + 2e^-$$
$$(LiI)_2 + e^- \rightarrow Li_2I^+ + I + 2e^-$$

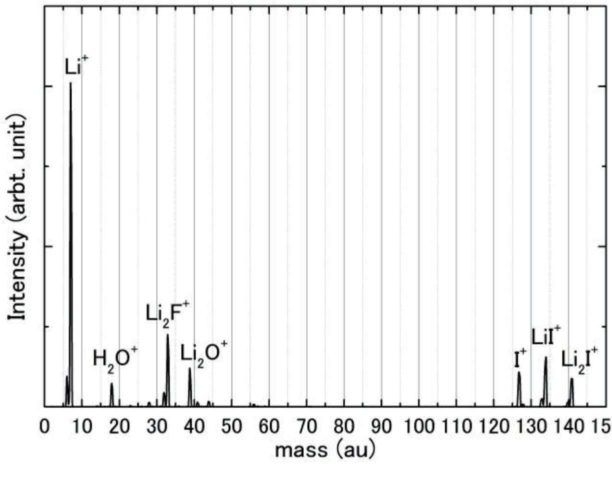

Fig. 1 Vapor mass spectrum of LiF-LiI system

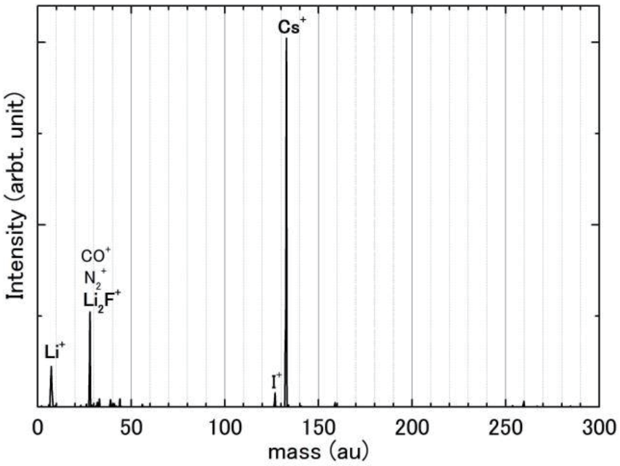

Fig. 2 Vapor mass spectrum of LiF-CsF system

Table 1 Gaseous species and its appearance potentials.

Ion species	appearance potential (eV)
Li^+	15.2
I^+	14.7
LiF^+	14.8
Li_2F^+	16.3
LiI^+	19.4
I_2^+	18.0
Cs^+	14.4
Cs_2F^+	14.0

Vapor pressures

The temperature dependences of vapor pressures for LiF-LiI and LiF-CsF systems are shown in Figs. 3 and 4, respectively. The vapor pressures were increased with temperature below 800 K. While, above 800 K, they were saturated because of the limit of the ion current detector. Li(g), LiF(g), $(LiF)_2$(g), LiI(g) and $(LiI)_2$(g) were the major volatile species in the LiF-LiI molten salts. It turned out that the fission product iodine evaporates easily together with lithium. For LiF-CsF pseudo-binary molten salt, Cs(g) and Li(g) were the major volatile species. Cesium evaporates independently unlike iodine.

Total vapor pressure of iodine species, LiI(g), at 800 K was larger than that of cesium species, Cs(g), in two orders of magnitude. Therefore, fission product iodine may be released easily from fuel salt.

2.3 Conclusion of Section 2

From measuring the vapor pressure over LiF-LiI and LiF-CsF molten salts using mass spectrometry, the following conclusions were obtained:

(1) The predominant vapor species over LiF-LiI molten salts were identified to be Li(g), LiF(g), $(LiF)_2$(g), LiI(g) and $(LiI)_2$(g).

(2) The predominant vapor species over LiF-CsF molten salts were identified to be Cs(g) and Li(g).

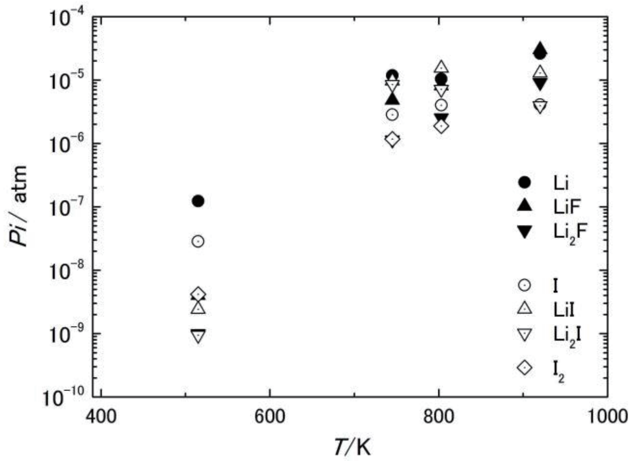

Fig. 3 Temperature dependencies of the vapor pressures corresponding to Li^+, LiF^+, Li_2F^+, I^+, LiI^+, Li_2I^+ and I_2^+ over LiF-70mol% LiI.

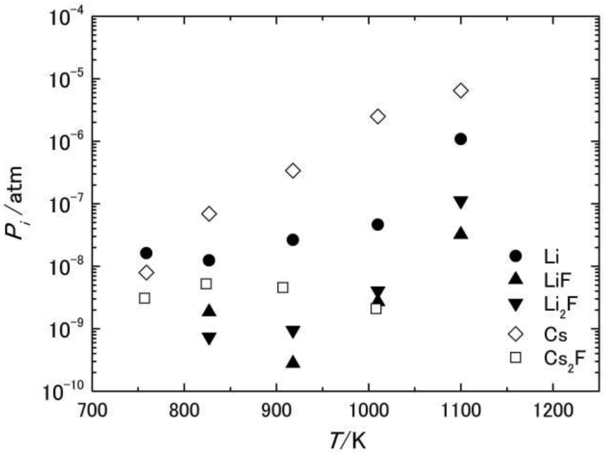

Fig. 4 Temperature dependencies of the vapor pressures corresponding to Li^+, LiF^+, Li_2F^+, Cs^+ and Cs_2F^+ over LiF-75mol%CsF.

(3) Iodine was more volatile than cesium.

3. Corrosion study of hastelloy-n alloy in molten salt

Corrosion tests were performed on Hastelloy-N specimen in FLiNaK molten salt at temperatures of 773 to 973K for 100 hours. After corrosion, cross sections of the specimens were observed and measured with scanning electron microscope (SEM) and energy-dispersive X-ray spectrometry (EDS). Effects of FPs and atmosphere were tested by adding CsI to molten salt and by exposure of molten salt to air, respectively.

3.1 Experimental

A rod specimen (1 × 1 × 20 mm) of nickel-based Hastelloy-N alloy (Ni-7Cr-16Mo-5Fe (wt%)) was prepared. The specimen surface was polished with sand paper (~#15000). Granules of FLINAK (LiF/NaF/KF ratio of 46.5:11.5:42 (wt%)) were also prepared. Figure 5 shows an illustration of the testing appaatus for molten salt corrosion. A 99.9% alumina crucible or a graphite crucible and a quartz tube were annealed at 1173 K with degassing in vacuum. All loading operations of the apparatus with a quartz tube, as shown in Fig. 5, were carried out in an argon-filled glove bag. The specimen and granules of molten salt were stacked in the alumina crucible or graphite crucible (4–5 mm ϕ × 27 mm). Some of the molten salt was stacked with cesium iodide at a molten salt/cesium iodide weight ratio of 10:1 to investigate the effect of FPs, which are to be generated in molten salt containing nuclear fuel or waste fuel, on the corrosion behavior of Hastelloy-N. A check valve was attached on top of the quartz tube after the crucible was loaded in the quartz tube. The closed quartz tube, which was filled with argon gas, was taken from the argon-filled glove bag. Some quartz tubes were filled with air to investigate the effect of air on corrosive attack of molten salt on Hastelloy-N in conditions simulating severe accidents. Afterward, the quartz tube was subjected to a corrosion test at high temperature by heating it in an electric furnace at 773 to 973 K for 100 h. After the test, the specimen was embedded in conductive resin, which was then cut with a cutting machine to observe the depth profile of corroded areas in cross sections. The cut surfaces were polished with sand paper (~#2000) and abrasive diamond grains (~0.25 μm) to prepare a milled surface for cross-sectional observation. The surface cross sections were observed with SEM, and surface chemical analysis was performed with EDS to obtain the depth profile of the corroded area. Thin-film samples for TEM observation were obtained from the corroded area by focused-ion-beam method. Corrosion products in the microstructure of the sample were observed. Electron diffraction method was performed in order to characterize corrosion products observed with TEM.

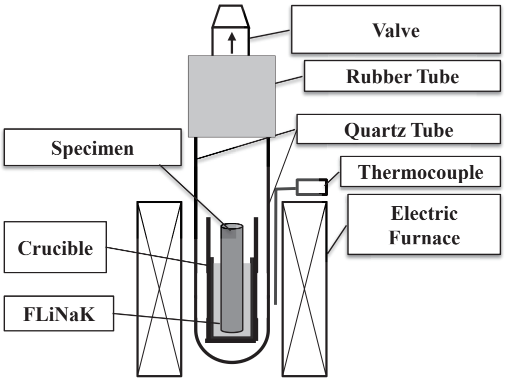

Fig.5: Illustration of the corrosion test apparatus

3.2 Results

Metallographic examination of Hastelloy-N tested at 773 K showed little evidence of corrosive attack other than shallow surface roughening (Fig. 6). There was no difference in the extent of corrosive attack on the surfaces of specimens in the alumina crucible and of those in the graphite crucible. The relative depth of attack was measured in the test done at 873 K. Figure 7 includes a SEM image and EDS mapping images for the specimens tested at 873 K. Chromium and molybdenum depletion down to a 10 μm depth were observed in the EDS mapping images. Subsurface voids were seen in the microstructure of the specimens. The grain size of the Hastelloy-N specimen was 20–30 μm, and there was no typical intergranular corrosion of the metallic surface. The depth of corrosion attack increased with increasing test temperature up to 923 K. Figure 8 shows SEM and EDS mapping images of a specimen immersed in molten salt and those of a specimen in molten salt–cesium iodide mixture at 923 K. The depth of corrosion attack in these specimens reached 50 μm, with the depth in the specimen in the graphite crucible being larger than that in the alumina crucible. There was no difference in the depths of corrosive attack between the specimen immersed in pure molten salt and that immersed in the molten salt–cesium iodide mixture. The average depth of corrosive attack was measured by metallographic examination. Figure 9 shows the temperature dependence of the depth of corrosive attack on the specimen surfaces exposed to various conditions. In order to compare the corrosion behavior of specimens in the molten salt solution against that of specimens reported in previous works, the corrosion rate was estimated from the measured depth of attack. When corrosion proceeds through an interfacial reaction, and when its reaction rate is proportional to the corrosion time, ~1.1 μm depth of corrosive attack is equivalent to ~1 mm/yr of uniform corrosion rate. TEM observation and EDS were performed on a section of corroded area by extracting a TEM sample from the deepest part of the site under corrosion attack. Some grains of molten fluoride salt such as those of the $K_3(Cr, Mo)F_3$ type with 0.81 ± 0.01 nm lattice parameter could be identified in the section of corroded area. These grains suggest that the solution of chromium-enriched or molybdenum-enriched molten fluoride salt accumulated on the corroded surface during a long period and that chromium and molybdenum did not quickly diffuse to the free surface during intergranular corrosion.

Figure 10 shows the depth of corrosive attack on the surface of specimens tested in argon gas and in air at 823 K. Apparently, corrosive attack in air was more extensive than that in argon gas. The depth of corrosion attack on the specimen immersed in pure molten salt was almost the same as that on the specimen in the molten salt–cesium iodide mixture (Fig. 10). This similarity suggests that corrosive attack in air significantly affected corrosion of Hastelloy-N in molten salt and that the synergistic effect of added FPs on corrosion in molten salt was negligible under these conditions.

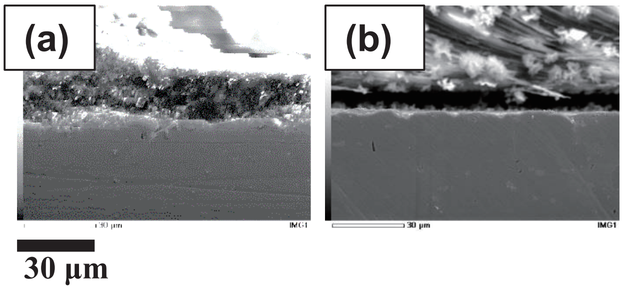

Fig. 6: Cross-sectional images of Hastelloy-N specimen immersed in molten salt at 773 K: (a) immersion test in an alumina crucible and (b) immersion test in graphite crucible.

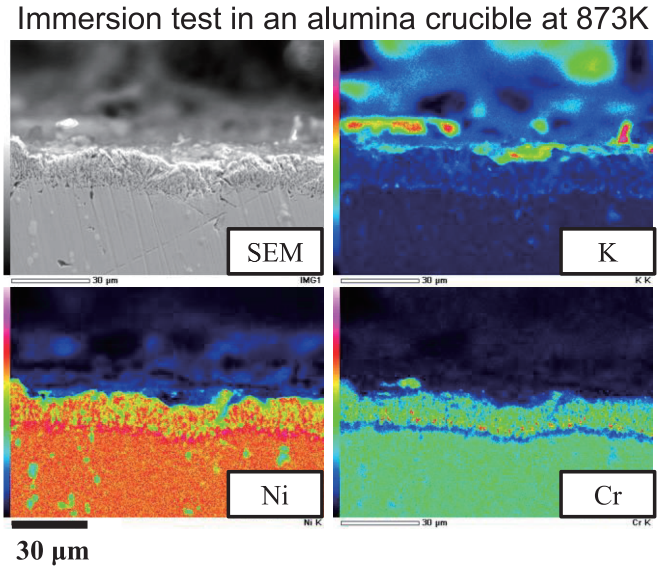

Fig. 7: Cross-sectional images of Hastelloy-N immersed in molten salt at 873 K. (a) SEM image and (b)–(d) element mapping images for K, Ni, and Cr, respectively, from EDS.

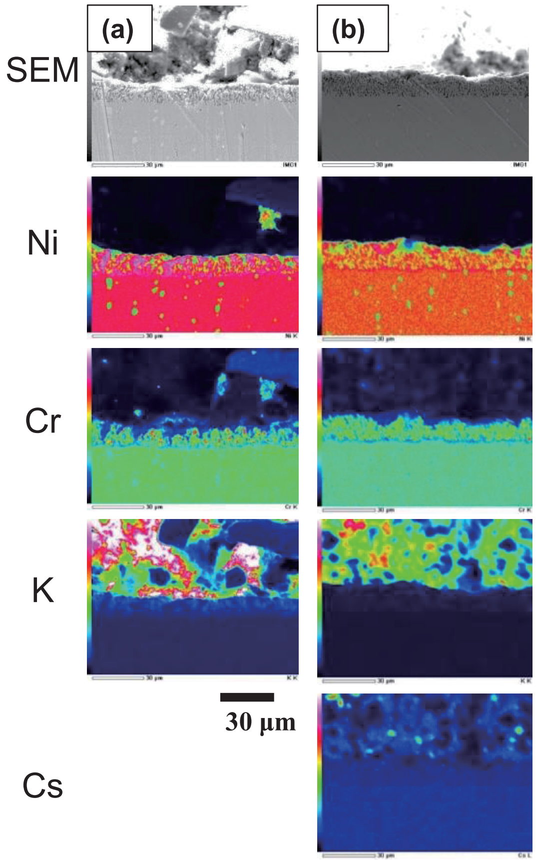

Fig .8: SEM and EDS mapping images of Hastelloy-N immersed in (a) molten salt and in (b) a molten salt–cesium iodide mixture tested at 923 K.

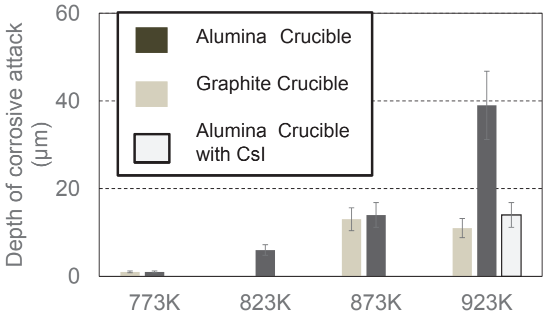

Fig. 9: Plot of the depth of corrosive attack versus test temperature.

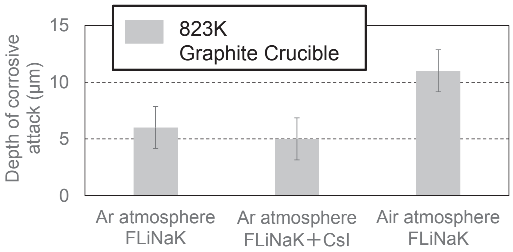

Fig. 10: Depth of corrosive attack on Hastelloy-N in pure molten salt under air (a) and under Ar gas (b) and on Hastelloy-N in a molten salt–cesium iodide-mixture under Ar gas (c).

3.3 Discussion

Fluoride salts constituting the molten salt are more thermodynamically stable than are fluorides of the metals constituting the structural alloys; thus, most structural alloys are stable in molten fluoride salts. Nickel, in particular, is relatively resistant to corrosion in molten fluoride salts. Previous works showed that impurities such as moisture could drastically accelerate corrosion via formation of hydrogen fluoride [4]. The effect of impurities in the molten fluoride salt on corrosion could be expressed in the following chemical reactions:

$2NaF + H_2O \rightarrow Na_2O + 2HF$

$2LiF + H_2O \rightarrow Li_2O + 2HF$

$2HF + Cr \rightarrow CrF_2 + H_2$

$NiF_2 + Cr \rightarrow CrF_2 + Ni$

In the case of FLiNaK, water could react with sodium fluoride and lithium fluoride in the salt and produce HF gas, which could leach chromium fluorides in the alloy into the salt. Impurities such as molybdenum or iron in salts for nickel-based matrixes can also promote dissolution of chromium into the salt. The present study differs from previous works in terms of the molten fluoride salt used (e.g., $LiF–BeF_2$ system vs. LiF–NaF–KF system) and the experimental procedure (e.g., static immersion test vs. thermal-convection loop test). However, the same tendency of corrosion behavior involving thermal interaction between molten fluoride salt and Hastelloy-N could be reproduced in this work.

The extent of corrosion of Hastelloy-N in molten salt under air was significantly greater than that in argon gas. Oxidation of molten fluoride salt probably caused loss of electrical neutrality and enhancement of the chemical activity of the surface reaction. In severe accidents such as leakage of molten salt into the primary coolant pipe, these lead to extensive, beyond-design-basis corrosion of the pipe surface. Addition of the FP cesium iodide to molten salt did not influence the corrosion attack on the microstructure of the specimen surface by molten salt. Some cesium remained in the molten salt phase at microstructural examination; only cesium or cesium iodide did not attack the surface directly. The synergistic effect of FPs such as cesium iodide on corrosion of the specimen surface in molten salt was not apparent; thus, the effect of the interaction between FPs and molten salt on corrosion of Hastelloy-N was negligible. However, tellurium or cesium telluride was reported to heavily attack the surface of stainless steel and of nickel-based alloy used in MFSR operation [14, 15]. The additional effect of tellurium in molten salt on corrosive attack on Hastelloy-N should thus be studied in the future.

Corrosion in molten salts includes dissimilar material corrosion in which differences in elemental activity between various materials in the molten salt drive deterioration. Corrosion of stainless steel in molten fluoride salt in graphite crucibles is significantly greater than that in stainless-steel crucibles [4]. In this work, there was no evidence of surface roughening of the alumina crucible after the immersion test, and the specimen was stable against corrosion in molten salt. The extent of surface corrosion of the specimen in molten salt in the graphite crucible was greater than that of the specimen in the alumina crucible, similar to the observation in a previous report [4, 15]. Graphite acts as a reductant for moisture and gas impurities in the molten salt solution and promotes the chemical interaction between the molten salt and specimen surface. Previous studies [16, 17] showed the acceleration of corrosion within corrosion capsules in a graphite crucible. This acceleration is due to the tendency of FLiNaK to cause chromium to take on multiple valence states, as well as the difference in chemical activities between the electronegative metal chromium in the alloy and the graphite crucible and components. When adding FPs in simulations of corrosion behavior in molten salt fuel containing nuclear waste, the effect of the crucible must be considered to ensure that the essential chemical interaction between molten salt and materials is not disrupted.

3.4 Conclusion of section 3

Effects of air on the corrosion of Hastelloy-N alloy in molten salt containing FP elements were investigated to evaluate the behavior of structural materials on a severe accident of MSR or FHR. Corrosion tests on Hastelloy-N in the molten fluoride salt FLiNaK were performed. The tests were performed at 773 to 923 K for 100 h in alumina crucible or graphite crucible under argon gas or under air. Metallographic examination of Hastelloy-N tested at 773 K showed little evidence of corrosive attack other than shallow surface roughening. The depth of corrosive attack, as well as the extent of chromium and molybdenum depletion, increased with increasing temperature. The extent of Hastelloy-N corrosion in molten salt under air was significantly greater than that in argon gas. The effect of cesium iodide added to molten salt on corrosion in a simulated test on the molten salt containing nuclear fuel or waste fuel was negligible. When adding FPs in corrosion test on molten salt fuel, the effect of the crucible must be considered so as not to disrupt the essential chemical interaction between the molten salt and material.

4. Overall summary

Source term for severe accident of MSRs was tackled by performing a vaporization study and corrosion study of fluoride molten salt. From the vaporization study, vapor species and vapor pressures of Cs- and I-containing species were identified and measured. From the corrosion study, effect of temperature, atmosphere (air, crucible) and FPs on corrosion attack of Hastelloy-N alloy by fluoride molten salt were determined. Results of this study suggest how to evaluate the source term for severe accident analysis of MSRs.

Acknowledgements

The study was partially supported by Chubu Electric Power Co.,Inc.

References

[1] K. Sridharan, "Understanding how materials corrode in nuclear reactors", Advanced Materials & Processes, 172, 17-20 (2014)

, C.W. Forsberg, P. Pickard, and P.F. Peterson, "Molten Salt-Cooled Advanced High Temperature Reactor for Production of Hydrogen and Electricity", Nucl. Technology, 144, 289-302 (2003)

[2] H.G. MacPherson, "Development of Materials and Systems for Molten Salt-Reactor Concept, Reactor Technology", 15, 136-155 (1972)

[3] K. Sridharan and T.R. Allen, "Corrosion in Molten Salts", "Molten Salts Chemistry: From Laboratory to Applications", Elsevier Inc. (2013)

[4] D. Wilson, "Corrosion Issues in Molten Fluoride Salts", ANS Annual Conference, Reno, NV, (2006)

[5] M.Knudsen, Ann. Physik. 28 (1909) 75.

[6] M.Knudsen, Ann. Physik. 29 (1909) 179.

[7] J.B.Mann, "Recent Developments in Mass Spectroscopy." K.Ogata, T.Hayakawa (EDs), Univ. of Tokyo, Tokyo, 1970, pp.814.

[8] P.Mahadevan, G.D.Manuson, J.K.Layton, C.E.Carlson, Phys.Rev. 140 (1965) A1407-1412.

[9] H.Yokokawa, S.Yamauchi, T.Matsumoto, Calphad 26 (2002) 155-166.

[10] J. H. DeVan and R. B. Evans III, "Corrosion behavior of reactor materials in fluoride salt mixtures", ORNL-TM-328 (1962)

[11] J.W.Koger, "Evaluation of hastelloy-N alloys after nine years exposure to both a molten fluoride salt and air at temperature from 700 to 560C", ORNL-TM-4189 (1972)

[12] L. C. Olsen, J. W. Ambrosek, K. Sridharan, M. H. Andersen and T. R. Allen, "Materials corrosion in molten LiF–NaF–KF salt", J. Fluorine Chem., 130 67-73 (2009)

[13] I. Ozeryanaya, "Corrosion of metals by molten salts in heat treatment process", Met. Sci. Heat Treat. 3 (1985) 184–188.